J-Band Transferred-Electron Oscillators

MICHAEL DEAN AND MICHAEL J. HOWES

Abstract—**An equivalent circuit for a *J*-band transferred-electron oscillator containing lumped and distributed elements is proposed. Using element values obtained independently, the equivalent circuit is shown to have broad-band applicability and is capable of explaining, in a strictly quantitative fashion, frequency saturation and the loss or absence of circuit-controlled oscillation. It is shown that the S4 type of encapsulation places severe constraints on the mounting structure and is not ideally suited to the *J*-band waveguide oscillator for optimum power-frequency characteristics over a broad band. The analysis of the full equivalent circuit given does, however, permit analytic solutions for important oscillator design parameters such as mounting post diameter, which enables simple post-mounted *J*-band oscillators that are free from frequency saturation and loss of circuit-controlled oscillation in the band to be easily designed.**

I. Introduction

CONSIDERABLE interest has been shown in recent years in the characteristics of mechanically and electronically tuned microwave oscillators based on the transferred-electron device. A simple and, therefore, attractive method of mounting the device in the case of a mechanically tuned waveguide oscillator is by means of a cylindrical post across the broad walls of the waveguide, as shown in Fig. 1(a) (the oscillation frequency is controlled by l). A variable reactance device can be introduced into the circuit in a similar manner if electronic tuning is also required. The mechanical simplicity of this type of oscillator, however, hides its electromagnetic complexity, and such an oscillator is often characterized by a number of effects that limit its potential usefulness.

Two of the most serious effects, particularly in the case of broad-band mechanically tunable oscillators, are "frequency saturation" and "hysteresis." Frequency saturation is an effect whereby the oscillation frequency remains substantially independent of the cavity length l and hysteresis is a bistable switching process between possible oscillation states of the system. Taylor *et al.* [1] have suggested that, in the absence of the device's inability to provide the necessary conductance, that is to match the real part of the impedance of the frequency determining network, frequency saturation may be due to a coaxial-type resonance between the top and bottom walls of the waveguide. The authors believe that this behavior is only important for short cavity lengths, where it is clear that even for an approximate description of the problem, TM modes in the vicinity of the post are required [2]. Tsai *et al.* [3] have proposed an equivalent circuit for *X*-band waveguide oscillators that accounts for many of the important characteristics of oscillators in that particular frequency band.

One of the present authors has indicated that a simple lumped/distributed equivalent circuit of the *J*-band waveguide oscillator could account for the gross features of the frequency tuning and power output characteristics [4]. This paper extends that work and proposes a model for the oscillator, which has a broad-band applicability and accounts for the detailed characteristics of such oscillators. Moreover, it is shown that analytic solutions for important design parameters may be extracted from a complete analysis of the oscillator.

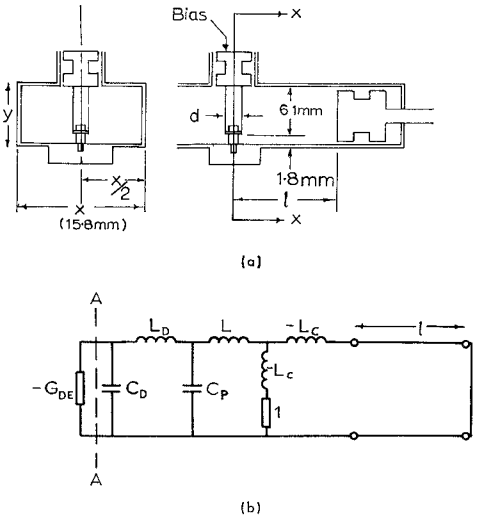

Fig. 1. (a) Mechanically tunable *J*-band (12.4–18 GHz) transferred-electron oscillator. (b) Proposed equivalent lumped/distributed-element circuit of oscillator shown in (a) ($C_D = C_{DE} + C_F$; $C_p = C_{pq} + C_{pp}$).

II. The Model

We have assumed that any model proposed for the oscillator must be capable of predicting the frequency of oscillation, the output power, and the tuning range (in the case of mechanically or electronically tuned oscillators) when the element values in the model have been determined by independent means. Thus it is not sufficient to show that the form of the model is essentially correct, and accurate numerical values must be assigned to each element in the model. The model used, however, is essentially linear and will not be capable of predicting effects due to the dynamic nonlinear behavior of the device.

The equivalent electrical network of the oscillator is obtained by dividing the microwave structure at convenient interfaces and considering equivalent network models for each part of the structure thus obtained. It is necessary, for continual network methods to be used, that all waveforms in the oscillator be assumed sinusoidal.

That part of the structure to the right of the mounting post [see Fig. 1(a)] might be represented in accordance with conventional microwave network theory by a stub of purely imaginary impedance $t = \tanh j\beta l$ ($\beta = 2\pi/\lambda g$) and a unity-value load resistor. The device mounting post is modeled by the T network described by Marcuvitz [5] and Lewin [6], a transformer being necessary if the post is not positioned in the center of the broad wall of the waveguide. This modeling

Manuscript received February 24, 1972; revised October 16, 1972.
The authors are with the Department of Electrical Engineering, University of Leeds, Leeds, England.

entails certain assumptions that have been fully discussed by others [7]. More accurate treatments of the post equivalent circuit are available [2], but their added complexity was not thought to be justified for this particular investigation, as explained previously. Note that the series elements in the T network are negative inductors ($-L_c$), a point often misinterpreted in the literature, while the parallel element is a positive or negative inductor (L) for broad-band equivalence. The devices used in this investigation were encapsulated in the S4 type of package, the equivalent circuit of which has been the subject of much debate [8], [9]. However, the majority of models that have been proposed in the literature may be reduced, to a first approximation, to a single L–C ladder network, where C_{pg} is the effective capacitance between the end caps of the package, L_D is the connecting lead inductance, and C_F is the fringing capacitance between the lead and the package walls.

The remaining part of the oscillator structure to be modeled is the device chip itself. With our assumption of approximately sinusoidal oscillations we may consider the device to be an arbitrary admittance

$$Y_{DE} = -G_{DE}(A, \omega) + jB_{DE}(A, \omega) \tag{1}$$

where G_{DE} and B_{DE} are, in general, a function of the frequency and amplitude of oscillation. The nature of this dependence does not concern us at present, since $|G_{DE}|$ will be determined by the conductance with which the device is loaded. It is clear that B_{DE} is capacitive, but its functional dependence on the frequency and amplitude of oscillation is not obvious. Therefore, we have assumed that $B_{DE}=\omega C_{DE}$, where C_{DE} is a constant capacitance, an estimate of which may be obtained from domain dynamics [14].

The resulting circuit model for the mechanically tuned transferred-electron oscillator is shown in Fig. 1(b). (C_p includes the additional capacitance between the bottom of the mounting post and the waveguide wall; C_{pg} results from the fact that, in general, the diameter of the mounting post is greater than the diameter of the top cap of the encapsulation.)

III. First-Order Analysis

The model described above is analyzed from the point of view of the active part of the device—G_{DE} [plane AA in Fig. 1(b)]. For the first-order analysis, small diameter ($d/x<0.1$) posts are assumed, which means that $L_c \simeq 0$ and L is constant in the equivalent circuit of the oscillator [5]. The admittance seen by $-G_{DE}$ is

$$Y_L(s, t) = G_L(s, t) + jB_L(s, t) \tag{2}$$

where s is the complex variable $\sigma+j\omega$ and $t=\tanh j\beta l$. In terms of the elements of the model,

$$Y_L(s, t) = \frac{Ls^2(1+t)B + (1+L_DC_Ds^2)(1+t) + Bst}{[1+t]As + Pt} \tag{3}$$

where the quantities A, B, and P are independent of t (see Appendix I). For steady-state oscillation we require that

$$B_L(s, t) = 0 \tag{4}$$

$$-G_{DE} + G_L(s, t) = 0. \tag{5}$$

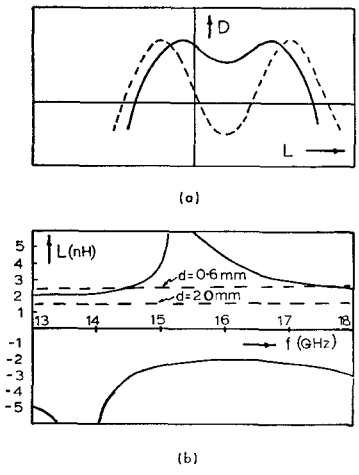

Fig. 2. (a) Dependence of the term $D=b^2-4ac$ in (6) on the value of the shunt inductive element L in the mounting post equivalent circuit. (b) Maximum value of mounting post inductance L (and hence minimum post diameter) that allows circuit-controlled oscillation versus frequency for the oscillator depicted in Fig. 1(a).

Assuming that $[[1+t]As+Pt]$ is finite, (4) results in a quadratic in the variable t which, assuming a lossless network and thus writing $t=j\tan\beta l$, yields the length of the cavity l explicitly in terms of ω at resonance as

$$l = \frac{1}{\beta}\arctan\left[\frac{-b \pm \sqrt{b^2 - 4ac}}{2a}\right] \tag{6}$$

where a, b, and c are functions of ω and the circuit element values and are defined in Appendix I.

There are two important features of (6): 1) double-tuning curves repeated at $n\lambda_g/2$ are predicted, i.e., (6) is satisfied for two values of l at the same frequency; 2) ranges of circuit element values that do not allow circuit-controlled oscillation at a particular frequency are predicted; i.e., for physically meaningful solutions to be possible, $D=b^2-4ac>0$ in (6). As an illustration of the significance of 2), the form of the dependence of D on the value of the inductive element L in the equivalent circuit is shown in Fig. 2(a) for constant ω and other element values. It is clear from this dependence that there are allowed bands of L (and hence post diameter) for resonance ($D>0$). In general, it is not possible to vary L while keeping the magnitude of other circuit element values fixed, since L and C_p are both dependent on the post geometry. However, for the small post diameters assumed in this first-order analysis, $C_p \simeq C_{pg}$ and is therefore constant. From characteristics such as those shown in Fig. 2(a), the critical values of L (those for which $D=0$) as a function of frequency may be obtained. For the S4 packaged devices used in this work, the circuit element values are given in Section VI ($C_p=0.2$ pF; $C_D=0.27$ pF; $L_D=600$ pH) and the corresponding allowed bands of post inductance for resonance in the frequency band 12–18 GHz are indicated in Fig. 2(b). Note that there is a maximum value of L that allows circuit-controlled oscillation throughout the band, 1.98 nH in this case and corresponding to a minimum post diameter of 1.5 mm.

The amplitude of oscillation is governed by (5), and thus for complete characterization of the system a knowledge of the real part of the impedance presented to the device chip at

resonance is required. If $Y_L(s, t)$ is regarded as

$$Y_L(s, t) = \frac{n_1 + m_1}{n_2 + m_2} \tag{7}$$

where n_1 and n_2 are odd polynomials in s and t and m_1 and m_2 are even polynomials in s and t, then at resonance $n_1 m_2 - m_1 n_2 = 0$ and

$$\text{Re}\,[Y(s, t)] = \frac{m_1}{m_2} = \frac{n_1}{n_2} \cdot \tag{8}$$

Hence the load presented to the device at resonance may be easily determined from (3) and (8).

The double-tuning curves predicted by (6) for this type of oscillator are not observed experimentally and to find an explanation for this it is necessary to investigate the stability of the oscillator, as discussed by others [3], [10]. It turns out that only one of the solutions of (6) corresponding to the positive sign represents a stable operating point, and the model, therefore, predicts a smooth tuning curve repeated at $n\lambda_g/2$ steps.

IV. Second-Order Analysis

It has been shown above that the use of small diameter posts, with a correspondingly high inductance, will considerably restrict the tuning range or prevent circuit-controlled oscillation. For practical oscillators, therefore, larger diameter posts are required and the assumption used in the first-order analysis, $L_c = 0$, is no longer valid. It is possible, however, to reduce the circuit obtained by including L_c to a similar form to that previously analyzed. Details of this procedure are discussed in Appendix II.

In order to further improve the validity of the model, the fact that the elements L and L_c in the model of the post are lumped representations of a distributed structure, and therefore are functions of frequency, has been taken into account. This has been achieved by ascertaining the nature of the variation of L and L_c using the work of Marcuvitz and taking a linear approximation to the variation as shown in Fig. 3. This linear dependence was subsequently used in the theoretical analysis of the oscillator.

Further evidence that the model described so far provides an adequate description of the oscillator is shown by its ability to explain the frequency saturation phenomenon discussed in the Introduction. Typical saturation curves are indicated in Fig. 4(a). We first note that this behavior will occur if at some point in the tuning range the model predicts a solution $l = \lambda_g/4$ (the frequency at this point corresponding to the saturation center frequency ω_{sat}). Referring to (6) we see that this condition is equivalent to $a = 0$, which for typical values of the circuit elements gives ω_{sat} within the frequency band investigated. In Section VI we shall show that, apart from predicting the occurrence of saturation, the model also predicts the detailed nature of the saturation curves and the variations of ω_{sat} with circuit parameters.

One aspect of frequency saturation that must be accounted for is the experimental observation that this phenomenon does not occur with unencapsulated devices in this type of microwave structure [12]. We shall now show that the proposed model does predict the absence of saturation in that case. For

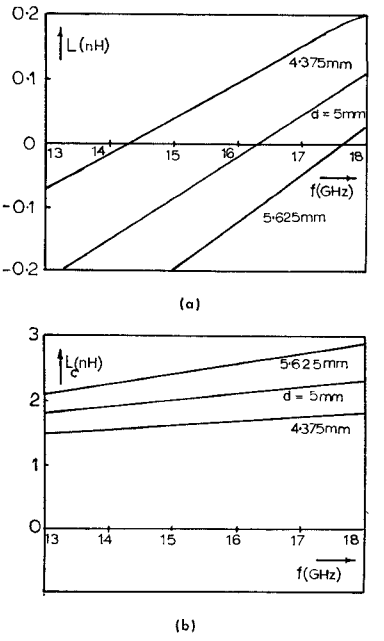

Fig. 3. Variation of magnitude of the elements in the mounting post equivalent circuit with frequency indicating the validity of assuming a linear approximation (i.e., $L = k_1 + k_2\omega$, $L_c = k_3 + k_4\omega$, where $k_{1,2,3,4}$ are functions of post diameter only).

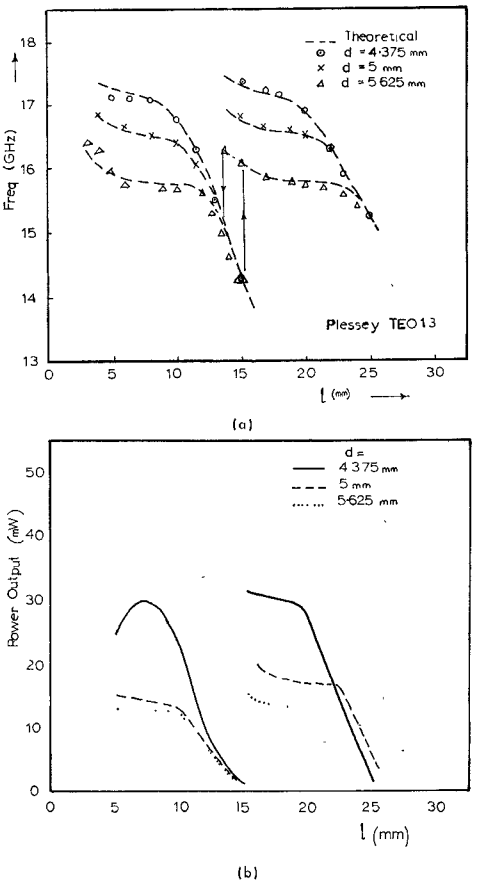

Fig. 4. (a) Mechanical tuning characteristics (oscillation frequency versus l) of the oscillator depicted in Fig. 1(a) for a number of different post diameters. Details of the devices are given in the insert. (b) Power output versus frequency for the same post diameters as in (a).

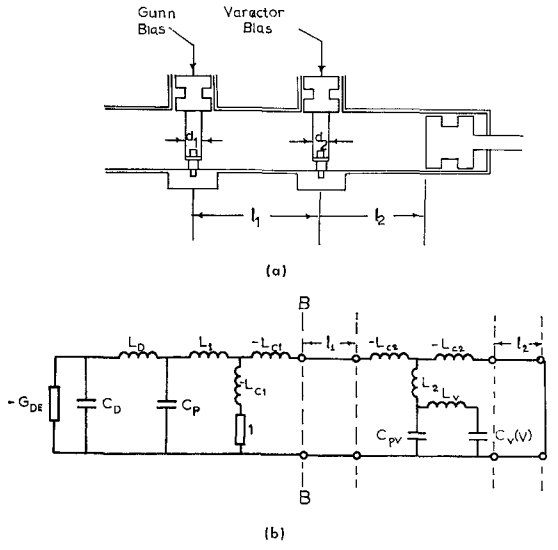

Fig. 5. (a) Varactor-tuned waveguide transferred-electron oscillator. (b) Proposed model of electronically tuned oscillator depicted in (a) (varactor loss not included).

unencapsulated devices, $L_D = 0$ and

$$a = L[L\omega_{sat}^2(C_D + C_p) - 1] + C_p + C_D = 0 \quad (9)$$

or, in unnormalized terms,

$$L = (C_p + C_D)Z_0^2 \Big/ \left(1 - \frac{\omega_{sat}^2}{\omega_0^2}\right) \quad (10)$$

where

$$\omega_0^2 = \frac{1}{L(C_D + C_p)}.$$

The minimum value of L for saturation occurs when $\omega_{sat}^2/\omega_0^2 \ll 1$, and therefore

$$L_{min} = (C_p + C_D)Z_0^2 \quad (11)$$

which when the extreme minimum value is taken for $C_p + C_D$ (i.e., 10^{-1} pF) results in $L_{min} = 16$ nH. This value of inductance is equivalent to a very thin post indeed (< 1 μm) and outside the normal range of post diameters. Thus the model does not predict the frequency saturation phenomenon with unencapsulated devices.

V. Electronically Tunable Oscillators

It has been shown, experimentally, that wide-band electronic tuning of waveguide-mounted transferred-electron oscillators is possible in reduced height cavities [13]. Such structures, however, are of low Q and result in oscillators characterized by poor FM noise performance.

Where noise performance is at a premium, standard height waveguide cavities must be used and an associated smaller tuning range accepted. Such a configuration is shown in Fig. 5(a), with the Gunn device and the tuning element (Schottky-barrier varactor diode) post mounted along the center line of the cavity. This structure is amenable to the same modeling technique as used for the mechanically tuned oscillator with the circuit model being that shown in Fig. 5(b). The analysis of this circuit is considerably simplified if the varactor is assumed lossless. The impedance seen to the right of BB is then purely imaginary and may be equated to t, solutions for which have been found in the previous analysis. The stability criteria of the previous analysis are also equally applicable.

VI. Experimental Techniques and Comparison of Characteristics of Practical Oscillators with Those Predicted by the Circuit Model

In order to test the validity of the circuit models presented, experimental studies of both mechanically and electronically tuned oscillators were carried out. Two cavities of the form shown in Figs. 1 and 5 were constructed with the mounting post diameters being variable by means of a set of brass sleeves.

Using conventional microwave techniques, curves of frequency and power output versus cavity length, in the case of the mechanically tuned oscillator, and frequency and power versus varactor bias, in the case of the electronically tuned oscillator, were taken for various post diameters. These characteristics are shown in Figs. 4(a) and (b) and 6 for the devices indicated in the figures.

To make a valid comparison with the characteristics predicted by the model described above, accurate values for the circuit elements must be obtained. The parameters L and L_c may be readily determined from the work of Marcuvitz and Lewin with the frequency dependence of these elements taken into account, as indicated in Section IV. The magnitude of the element C_p has been determined by several methods. First, an approximation to its value was obtained using the quasi-static approximation

$$C_p = C_{pg} + \left[\frac{\epsilon_0 \pi}{2} \ln \frac{L}{a}\right] d + \frac{\epsilon_0 \pi}{4a}[d^2 - d'^2] \quad (12)$$

where d is the post diameter, d' is the diameter of the S4 package, a is the distance between the bottom of the post and the waveguide wall, L is the post length, and C_{pg} (0.14 pF) is the capacitive element associated with the unmounted packaged device. The variation of C_p with post diameter as predicted by (12) is compared with measurements made at 1 MHz using a Wayne Kerr B201 bridge in Fig. 7. These results, along with the results from other works, indicate that (12) adequately describes the variation of C_p with post diameter. The value of the package lead inductance for the encapsulate used is known to be in the range 580–650 pH, and a value of 600 pH has been used in this work. The only other circuit element value required is the device capacitance C_D. Using the theoretical and experimental results of other workers [14] it appears that $C_D = 0.27$ pF for the particular devices used, and it is also significant that this value yields the correct value of saturation frequency when the values of C_p shown in Fig. 7 are used.

The theoretical tuning curves for the mechanically tuned oscillator may now be obtained from (6) using the element values as determined above. Fig. 4(a) indicates excellent agreement between the tuning curves as predicted by the model and the experimental curves. It is clear that the model completely explains the frequency saturation phenomenon and the variation of saturation frequency with post geometry. The experimental tuning [Fig. 4(a)] curves also exhibit hysteresis (the vertical lines indicating abrupt transitions in frequency and their direction). This behavior has been reported at lower frequencies by others [3], [7] and has been fully discussed in [3] (also see Edson [11] and Kurokawa [10]).

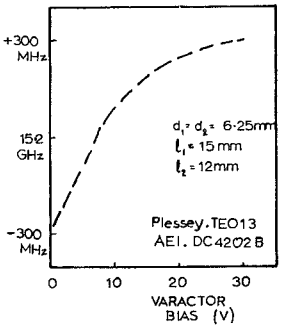

Fig. 6. Dependence of oscillation frequency of electronically tuned oscillator on varactor bias voltage (details of devices used are given in the insert).

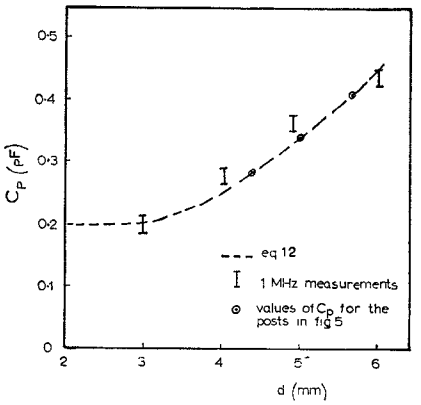

Fig. 7. Comparison of the variation of package capacitance C_p with the post diameter using the various methods indicated in the text.

TABLE I

COMPARISON OF PREDICTED AND EXPERIMENTAL OSCILLATION FREQUENCY WHEN THE s/c IN FIG. 1(a) IS REPLACED BY A MATCHED LOAD

d_2 (mm)	freq. exp. (GHz)	freq. theor. (GHz)
4·375	17·33	17·10
5·0	16·74	16·70
5·625	15·93	15·95

Another check on the quantitative validity of the model can be made by replacing the variable s/c with a matched load. The distributed element $jZ_0 \tan \beta l$ in the model [Fig. 1(b)] is now replaced by a resistive element Z_0. The theoretical value of oscillation frequency obtained from this circuit as compared with experimental values is shown in Table I for various post diameters. Again, excellent agreement is apparent.

In the case of the electronically tuned oscillator, the equivalent circuit shown in Fig. 5(b) has been analyzed to yield the center frequency and tuning range for the full range of variactor bias. The results of this analysis are depicted in Table II, where it is shown that the experimental and theoretical center frequencies agree to 2 percent and the tuning ranges to 20 percent. It is believed that the discrepancy in the tuning ranges is due to the failure to take into account varactor loss in the model.

TABLE II

COMPARISON OF PREDICTED AND EXPERIMENTAL TUNING RANGES AND CENTER FREQUENCY FOR THE ELECTRONICALLY TUNED OSCILLATOR SHOWN IN FIG. 5(a)

$d_1 = 625$ mm $\quad d_2 = 6{\cdot}25$ mm

$l_1 = 15$ mm $\quad l_2 = 12$ mm

$C_v(V=0) = 0{\cdot}72$ pF; $C_v(-30V) = 0{\cdot}12$ pF

	CENTRE FREQ.	TUNING RANGE
EXP	15·2 GHz	600 MHz
THEORY	15·35 GHz	710 MHz

VII. Conclusions

It has been shown that the proposed lumped/distributed-element equivalent circuit of a J-band Gunn oscillator operating in a post-mounted waveguide structure is capable of accounting for the detailed characteristics of such oscillators in a quantitative fashion. It is proposed, therefore, that the equivalent circuit may be used to develop accurate design procedures in order to optimize the tuning range (electronic and mechanical) and power output of such oscillators. In particular, it is clear that the S4 type of package places constraints on the mounting post diameter in order to achieve circuit-controlled resonance over a specific band of frequencies, and the analysis presented may be used to determine the minimum post diameter appropriate to a specific frequency band. Alternatively, the analysis may be applied to the problem of designing a package that may eliminate the problems of frequency saturation and switching, which are characteristic of simple post-mounted Gunn oscillators operating at frequencies greater than 10 GHz.

We have shown that the frequency saturation phenomenon observed in J-band oscillators may be removed from the band by increasing the post diameter and/or decreasing the capacitance C_p associated with the mounted package by, for example, lifting the device off the waveguide wall. This latter remedy has been suggested by others, but for fundamentally different reasons [1].

Appendix I

Referring to Fig. 1(b) we see that the admittance of the circuit as viewed from the plane AA is given in terms of the complex variables s and t as

$$Y_L(s,t) = \frac{Ls^2(1+t)B + (1 + L_D C_D s^2)(1+t) + Bst}{(1+t)As + Pt} \quad (13)$$

where

$$B = C_D + C_p + C_D L_D C_p s^2$$
$$A = L + L_D + L L_D C_p s^2$$
$$P = 1 + L_D C_p s^2.$$

For steady-state oscillation,

$$B_L(s,t) = 0 \quad (14)$$
$$-G_{DE} + G_L(s,t) = 0. \quad (15)$$

Equation (14) implies that either

$$(Ast)(Ls^2tB + t(1 + L_DC_Ds^2)) - (As + Pt)(Ls^2B + 1 + L_DC_Ds^2 + Bst) = 0 \quad (16)$$

or

$$(1 + t)As + Pt \rightarrow \infty. \quad (17)$$

Ignoring the solution given by (17) [since this also gives $G_L(s, t) = 0$, and therefore zero power output], (16) is of the form

$$a(s)t^2 + b(s)t + c(s) = 0. \quad (18)$$

Letting $s \rightarrow j\omega$ and $t \rightarrow jt$,

$$\begin{aligned} a(j\omega) &= A\omega(L\omega^2B + \sigma) + PB\omega \\ b(j\omega) &= P(L\omega^2B + \sigma) + AB\omega \\ c(j\omega) &= A\omega(L\omega^2B + \sigma) \\ \sigma &= L_DC_D\omega^2 - 1. \end{aligned} \quad (19)$$

The solutions of (18) are given by

$$t = \tan \beta l = (-b \pm \sqrt{b^2 - 4ac})/2a. \quad (20)$$

For physically meaningful values of cavity length l, we require that $b^2 > 4ac$ or

$$[1 - 2A\omega(L\omega^2B + \sigma)][1 + 2A\omega(L\omega^2B + \sigma)] = 0 \quad (21)$$

which may be written as a quartic in L, and hence yields four critical values of L for constant ω and other system parameters, at which the discriminant of (20) is zero. Similar equations may be derived for the other parameters of the circuit. In practice, L and C_p are not independent, since both are functions of the post diameter. However, for small posts the major portion of C_p is contributed by the package that is constant. The conditions for circuit-controlled oscillation may be examined further by determining the first and second partial derivatives of D with respect to L.

$\partial D/\partial L = 0$ for three values of L, i.e.,

$$\begin{aligned} L_a &= -L_D/P \\ L_b &= -\sigma/\omega^2B \\ L_c &= (L_a + L_b)/2. \end{aligned} \quad (22)$$

These values of L yield the following values of D and $\partial^2D/\partial L^2$:

$$\begin{aligned} D(L_a) &= 1 & \left(\frac{\partial^2 D}{\partial L^2}\right)_{L_a} &= -8\omega^2 \\ D(L_b) &= 1 & \left(\frac{\partial^2 D}{\partial L^2}\right)_{L_b} &= -8\omega^2 \\ D(L_c) &= 1 - \frac{1}{4\omega^2P^2Y^2} & \left(\frac{\partial^2 D}{\partial L^2}\right)_{L_c} &= 8\omega^2. \end{aligned} \quad (23)$$

It follows, therefore, that the quantity $D(L)$ has two maxima at L_a and L_b and one minimum at L_c midway between the maxima. Also, $D(L_a)$ and $D(L_b)$ are always positive, while $D(L_c)$ may be negative or positive. $D(L)$ is thus of the form shown in Fig. 2(a) and defines the allowed bands of L that permit circuit-controlled oscillation.

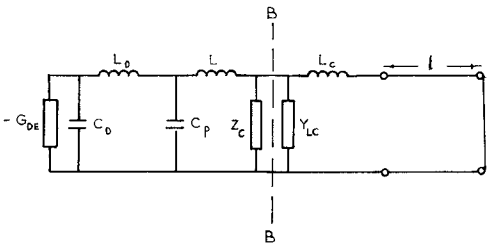

Fig. 8. Simplification of equivalent circuit in Fig. 1(b) for second-order analysis.

Appendix II

To analyze the oscillator circuit when the assumption $L_c = 0$ is not valid, it is convenient to regard the series combination of the load and L_c in Fig. 1(b) as a shunt combination of a load Z_c and a lossless admittance Y_{Lc}, where

$$Z_c = 1 + \omega^2L_c^2 \qquad Y_{Lc} = \frac{+j\omega L_c}{1 + \omega^2L_c^2}. \quad (24)$$

Renormalizing with respect to Z_c we arrive at the circuit shown in Fig. 8. The circuit to the right of plane BB is lossless and may be represented by the single impedance $j\tau_c$. The circuit is now identical to that analyzed above except that τ_c replaces $j\beta l$ and all elements are normalized with respect to $Z_c \times Z_0$ rather than Z_0. Therefore, for steady-state oscillation,

$$\tau_c = \frac{-b' \pm \sqrt{b'^2 - 4a'c'}}{2a'} \quad (25)$$

where a', b', and c' are identical to a, b, and c when all circuit elements are renormalized. The product βl may be extracted from τ_c as

$$\beta l = \arctan (Z_c\tau) \quad (26)$$

where

$$\tau = \frac{\tau_c}{(1 + Y_c\tau_c)} - \omega L_c.$$

Acknowledgment

The authors would like to acknowledge the support of the Scientific Research Council. One of the authors (M. Dean) also wishes to acknowledge the support of the British Broadcasting Corporation.

References

[1] B. C. Taylor, S. J. Fray, and S. E. Gibbs, "Frequency-saturation effects in transferred electron oscillators," *IEEE Trans. Microwave Theory Tech. (Special Issue on Microwave Circuit Aspects of Avalanche-Diode and Transferred Electron Devices)*, vol. MTT-18 pp., 799–807, Nov. 1970.

[2] R. L. Eisenhart and P. J. Khan, "Theoretical and experimental analysis of a waveguide mounted structure," *IEEE Trans. Microwave Theory Tech.*, vol. MTT-19, pp. 706–719, Aug. 1971.

[3] W. C. Tsai, F. J. Rosenbaum, and L. A. MacKensie, "Circuit analysis of waveguide-cavity Gunn-effect oscillator," *IEEE Trans. Microwave Theory Tech. (Special Issue on Microwave Circuit Aspects of Avalanche-Diode and Transferred Electron Devices)*, vol. MTT-18, pp. 808–817, Nov. 1970.

[4] M. J. Howes, "Circuit consideration in the design of wide-band tunable transferred-electron oscillators," *IEEE Trans. Electron Devices*, vol. ED-17, pp. 1060–1067, Dec. 1970.

[5] N. Marcuvitz, *Waveguide Handbook*. New York: McGraw-Hill, 1951.

[6] L. Lewin, *Advanced Theory of Waveguides*. London, England: Iliffe, 1951.

[7] C. P. Jethwa and R. L. Gunshor, "Circuit characterisation of wave-

guide-mounted Gunn-effect oscillators," *Electron Lett.*, vol. 7, no. 15, p. 433, 1971.
[8] W. J. Getsinger, "The packaged and mounted diode as a microwave circuit," *IEEE Trans. Microwave Theory Tech.*, vol. MTT-14, pp. 58–69, Feb. 1966.
[9] R. P. Owens and D. Cawsey, "Microwave equivalent-circuit parameters of Gunn-effect-device packages," *IEEE Trans. Microwave Theory Tech. (Special Issue on Microwave Circuit Aspects of Avalanche-Diode and Transferred Electron Devices)*, vol. MTT-18, pp. 790–798, Nov. 1970.
[10] K. Kurokawa, "Some basic characteristics of broadband negative resistance oscillator circuits," *Bell Syst. Tech. J.*, vol. 48, p. 1937, 1969.
[11] W. A. Edson, *Vacuum Tube Oscillator*. New York: Wiley, 1953.
[12] B. C. Taylor and M. J. Howes, "LSA operation of GaAs layers in large-scale tunable microwave circuits," *IEEE Trans. Electron Devices*, vol. ED-16, pp. 928–934, Nov. 1969.
[13] B. J. Downing and F. A. Myers, "Broadband (1.95 GHz) varactor-tuned X-band Gunn oscillator," *Electron. Lett.*, vol. 7, no. 14, p. 107, 1971.
[14] G. Hobson, "The equivalent circuit of a Gunn effect device," *Proc. Microwave Opt. Generation Amplification*, p. 314, 1966.

Noise in Single-Frequency Oscillators and Amplifiers

REIDAR L. KUVÅS

Abstract—**A generalization of previous oscillator noise analyses has been developed to permit reliable noise characterization of active nonlinear devices. Effects due to sideband correlation in the equivalent noise source are included. A rotating wave approximation (RWA) developed by Lax is used in obtaining the amplitude and phase noise spectra. Conditions are given for phase stabilization of free-running oscillators and for minimum phase noise in phase-locked oscillators and amplifiers. Stability criteria, discussion of spurious sidetones, and effects of a noisy synchronizing signal are given. The noise measure is used to obtain alternative expressions for the noise spectra and the carrier-to-noise ratios of locked oscillators and amplifiers. It is shown that the noise power gain of AM fluctuations is usually much lower than the corresponding gain for FM noise. The theory should be useful in optimizing the noise performance of nonlinear RF generators, such as IMPATT, BARITT, and Gunn diode oscillators.**

I. Introduction

THE NOISE FIGURE is a convenient quantity for specifying the noise characteristics of linear amplifiers, since it is uniquely related to the signal-to-noise ratio (SNR). The situation is more complex in oscillators and large-signal amplifiers. The inherent nonlinearities in such components may cause the signal and noise to transform differently. As a result, the SNR can be sensitive to the operating parameters of the nonlinear system in addition to the strengths of the noise sources. Thus noise characterization of oscillators and large-signal amplifiers is a nontrivial problem.

An informative study on noise in free-running and phase-locked oscillators was presented by Kurokawa [1]. This study gives detailed results for the spectra of the amplitude and phase noise (the spectra for the free-running case were originally derived by Edson [2]), for the possible improvement in FM noise by phase locking, and for the adverse effects of a noisy synchronizing signal. In addition, Kurokawa's theory describes the asymmetry of the noise spectrum and an expected increase in the phase noise when the synchronizing frequency in locked oscillators differs from the free-running frequency. This initial study did not include the frequency dependence of the elements in the equivalent circuit and the derivative of the reactance with respect to the level of operation. These restrictions were removed in a subsequent analysis [3].

The rotating wave approximation (RWA) employed by Lax [4] is very effective in permitting a general but simple formulation of the oscillator noise problem. He derived conditions for decoupling amplitude and phase fluctuations that give a minimum phase noise. A simple analytic expression was obtained for the linewidth, even in the case when these conditions were not met. Important results were given for amplitude fluctuations.

Advantage will be taken of the RWA method in our derivations to obtain generalized results for locked oscillators and amplifiers. For completeness, some of the results obtained by Lax for free-running oscillators will be rederived.

Previous noise analyses have not considered the possibility of correlation between the sidebands of the noise sources. In Appendix I it will be shown that mixing effects in nonlinear systems in general will introduce finite correlation factors. In fact, full sideband correlation has been calculated for the specific case of an IMPATT diode in large-signal operation [5]. Therefore, the present analysis has been generalized to include effects of correlated noise sidebands.

II. Circuit Model

The temporal variation of the RF signal in a well-designed single-frequency oscillator or amplifier is close to being a pure sinusoid. Thus the RF circuit current $I(t)$ of instantaneous amplitude $A(t)$ and phase $\phi_1(t)$ can be written:

$$\begin{aligned} I(t) &= A(t)\cos[\omega_0 t + \phi_1(t)] \\ &= A_0[1 + a(t)]\cos[\omega_0 t + \phi_0 + \phi(t)] \end{aligned} \quad (1)$$

where ω_0 is the signal frequency and A_0 and ϕ_0 represent the amplitude and the phase in the noise-free case. In the presence of noise, slow variations are introduced into the amplitude and phase, which in (1) are described by the normalized amplitude fluctuation $a(t) = [A(t) - A_0]/A_0$ and the phase fluctuation $\phi(t) = \phi_1(t) - \phi_0$, respectively.

The nonlinear behavior of oscillators and large-signal amplifiers in general introduces some higher harmonic content

Manuscript received December 20, 1971; revised August 31, 1972.
The author is with Bell Telephone Laboratories, Inc., Reading, Pa. 19604.